

Corrosion Properties of F82H in Flowing High Temperature Pressurized Water

Motoki NAKAJIMA, Takanori HIROSE, Hisashi TANIGAWA, Mikio ENOEDA

Japan Atomic Energy Agency, Rokkasho, Aomori, Japan

(Received: 30 September 2014 / Accepted: 19 January 2015)

This work reports the effects of water flow and dissolved oxygen (DO) on corrosion behavior of reduced activation ferritic/martensitic steel, F82H. The corrosion tests were performed in high temperature pressurized water by using a test apparatus for rotated disk sample. All of specimens showed weight gains after static corrosion tests up to 500 h. However, the rotated disk showed weight losses except for test in the water with DO=8 ppm, and the weight loss was significant with lowering DO concentration.

Keywords: Reduced activation ferritic/martensitic steel, Corrosion, High temperature pressurized water, Flow accelerated corrosion, Test blanket module, Dissolved oxygen

1. Introduction

Water-cooled blanket is an attractive concept for its compactness and its compatibility with the conventional technologies for pressurized water reactor (PWR) [1-3]. For blanket application, the structural material is required to be as thin as possible for tritium breeding. On the other hand, the pressure tightness is required to withstand 15 MPa of internal pressure. Therefore it is necessary to understand the corrosion mechanism in high temperature pressurized water. However, the corrosion data of reduced activation ferritic/martensitic steel (RAFM), F82H is limited in high temperature pressurized water condition. Shiba et al. reported the weight change of F82H located in autoclave with dissolved oxygen of 1 ppm at temperatures ranging from 493 K to 563 K in the pressure of 10 MPa [4]. The results demonstrated that the specimen lost weight at temperatures below 533 K but gained weight at temperatures over 533 K. And they also reported that corrosion properties of F82H were almost same as that of 12% chromium steel, HT-9. Hirose et al. measured the weight change behavior of F82H in super critical pressurized water up to 1000 h [5]. The weight simply increased with surface oxidation and the weight change of F82H was almost same as commercial 9% chromium steels. In either case, they reported the corrosion properties in static water condition. However, the maximum flow rate of ITER-TBM is planning to 6 m/s [6]. Therefore, it is essential to understand the corrosion properties in flowing high temperature water condition.

This work reports results of corrosion tests on a reduced activation ferritic/martensitic steel, F82H as a *author's e-mail:nakajima.motoki@jaea.go.jp*

structural material for the blanket. Moreover, the effects of water flow and dissolved oxygen (DO) in the test water on corrosion properties were investigated using rotating disk specimen in autoclave.

2. Experimental procedure

The material used in this study was a RAFM steel, F82H (Fe-8Cr-2W-0.2V-0.04Ta-0.1C). The corrosion test using a rotated disk specimen ($\phi 100$ mm x 5 mm) was performed in the autoclave with rotation speed of 1000 rpm. The circumferential velocity on the specimen edge was 5 m/s. The coupon type specimen (20 x 20 x 1.0 mm³) was used for static corrosion test. All specimens were mirror finished by a buff polishing. The DO concentrations in the inlet water were 20 ppb, 1 ppm, 3 ppm and 8 ppm. The corrosion tests were conducted at 573 K with the pressure of 15 MPa. The corrosion tests were performed under testing time ranging from 28 h to 500 h. Before and after the corrosion test, the specimen weight was measured by using a precision balance. Corrosion products were examined on the specimen surface and cross-section using scanning electron microscopy (SEM), X-ray diffraction (XRD) spectrometry, and electron probe micro-analyzer (EPMA).

3. Results and Discussion

Figure 1 shows the weight change of coupon type specimen plotted as a function of testing time. All of the specimens gained weight after static corrosion tests up to 500 h. It seems that their increases follow the parabolic law. As shown in this figure, the DO concentration has no

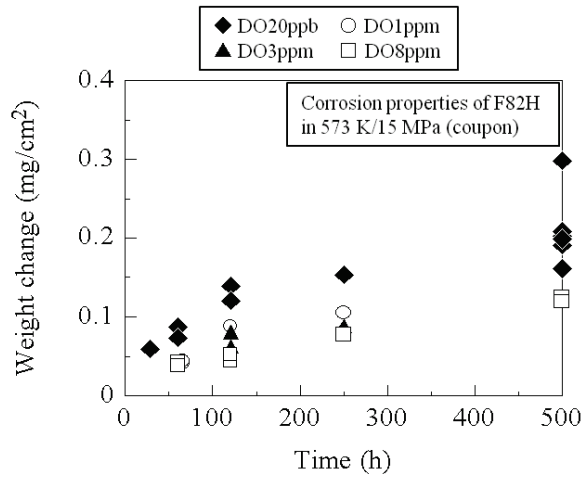


Figure 1 Weight change of coupon type specimen plotted as a function of time.

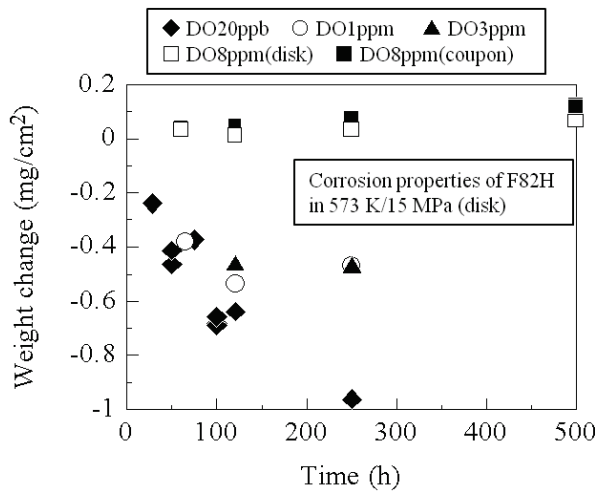


Figure 2 Weight change of rotated disk specimen plotted as a function of time. The result of coupon type specimen measured on DO 8 ppm was also plotted in this figure.

significant influence on the corrosion rate. On the contrary, as shown in figure 2, rotated disks lost weight except for the test with DO 8 ppm, and the weight loss became significant with lowering DO concentration. Additionally, there were no significant difference between the weight change of coupon type specimen and that of disk type specimen at DO 8 ppm condition.

Figure 3 shows the SEM micrographs of the specimen surface after corrosion test. All of the specimens tested in the static water, the block like oxides are observed on each sample. The particle size of 20 ppb sample was significantly enlarged. The oxide morphology of the rotated disk tested in the water with 20 ppb DO was quite different from the others. Although the oxide particles were not observed on the surface of DO 20 ppb, the block like oxide particles were formed in DO contents greater than 1 ppm. These results suggested that the oxide which was formed on the coupon specimen of 20 ppb was lost by the water flow. It can be speculated that the oxide was lost as a results of dissolution and/or exfoliation.

Figure 4 shows the results of XRD spectrometry on specimen tested in static water. The results indicated that the surface oxide of 20 ppb specimen was identified as Magnetite (Fe_3O_4). With increasing DO concentration, the dominant surface oxide was changed from Fe_3O_4 to Hematite (Fe_2O_3). This change of surface oxide was seemed to be attributable to increase the corrosion potential which caused by the increase of DO concentration. XRD patterns of rotated disk sample were shown in Fig. 5. It can be seen that the Fe_2O_3 peak disappeared under the water flow condition. Since it has been well known that the solubility of Fe_2O_3 was quite smaller than that of Fe_3O_4 , the surface oxide of higher DO concentration could be regarded as Fe_2O_3 [7].

Figure 6 shows the EPMA mapping of cross section of rotated disk specimen. The observation was performed on the edge of the disk specimen ($r=50$ mm). The elemental mappings of 1 ppm, 3 ppm and 8 ppm showed

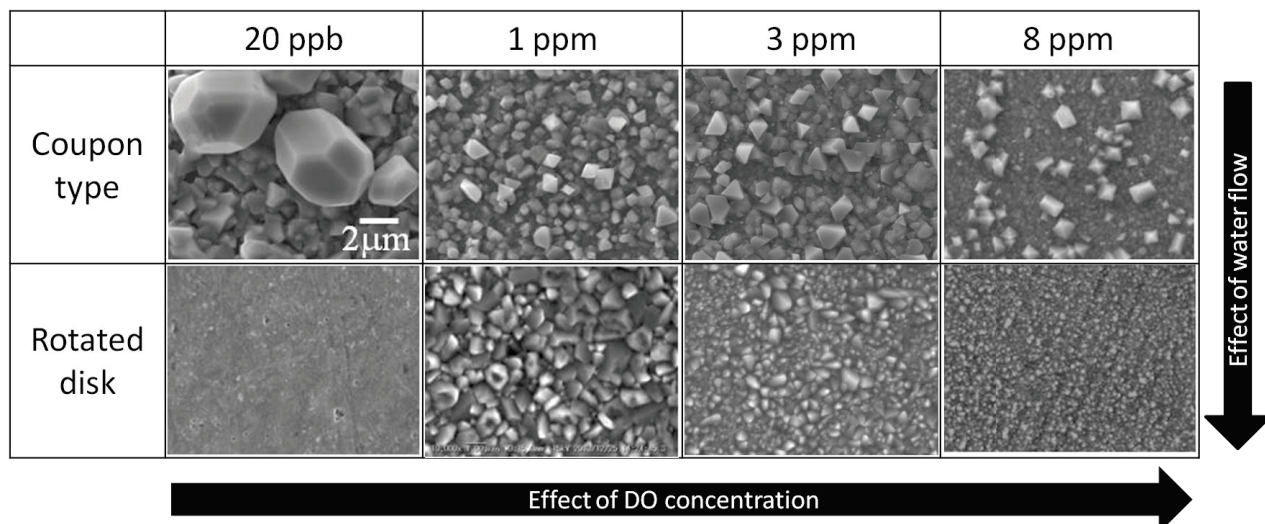


Figure 3 SEM micrographs of the specimen surface after corrosion test for 250 h.

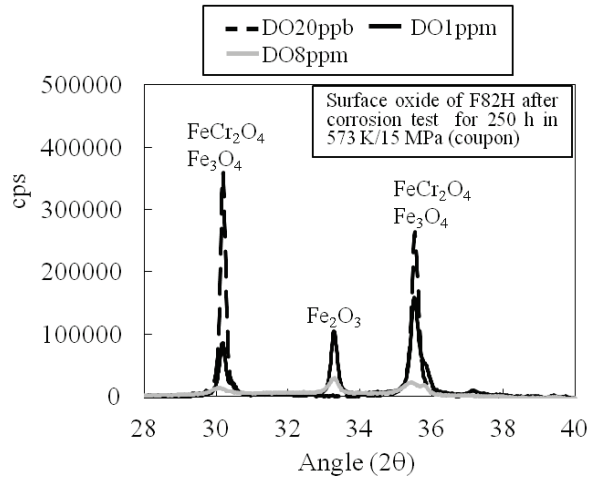


Figure 4 XRD patterns measured on DO 20 ppb, 1 ppm and 8 ppm of coupon type specimen.

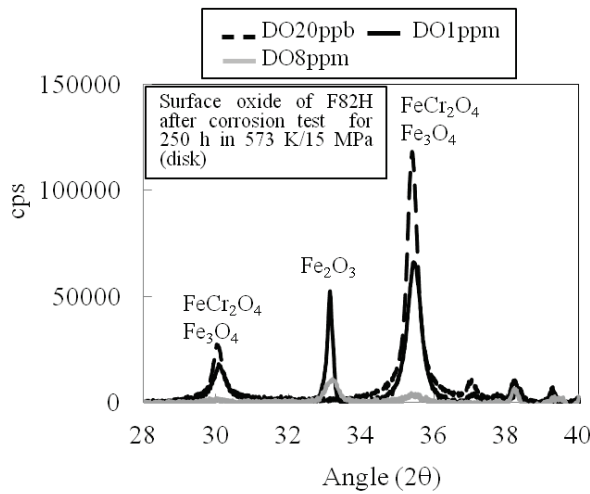


Figure 5 XRD patterns measured on DO 20 ppb, 1 ppm and 8 ppm of rotated disk specimen.

the outer block oxide was Fe oxide and the inner oxide (iron-poor layer) was chromium rich oxide. According to the XRD results of rotated disk samples, the inner oxide was identified as the FeCr_2O_4 . Comparing the thickness of iron-poor layer, the thickness was increased with decreasing the DO concentration. This iron-poor layer should be formed as a result of dissolution of Fe ions. Therefore, it can be concluded that the weight loss of the disk specimen was caused by the Fe ion dissolution from base metal. Considering the results of SEM observation and EPMA mapping, relatively smaller iron-poor layer was observed on the specimen which was formed Fe_2O_3 on the surface. These results suggest that the Fe_2O_3 may act as the protective oxide for Fe ion transport. Therefore, Fe_2O_3 ratio in the oxide was estimated from the results of XRD spectra measured on the coupon type specimen. The $\text{Fe}_2\text{O}_3/\text{Fe}_3\text{O}_4$ ratio was determined by dividing the peak value of XRD of

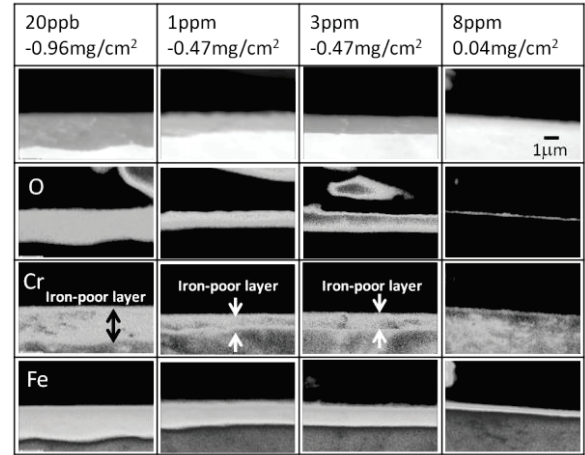


Figure 6 EPMA element map (O, Cr, Fe) measured on the cross section of rotated disk specimen ($r=50$ mm) after corrosion test for 250 h.

Fe_2O_3 by that of Fe_3O_4 . DO dependency of $\text{Fe}_2\text{O}_3/\text{Fe}_3\text{O}_4$ ratio was shown in figure 7. $\text{Fe}_2\text{O}_3/\text{Fe}_3\text{O}_4$ ratio has a tendency to increase with increasing the DO concentration. It was considered that the increase of $\text{Fe}_2\text{O}_3/\text{Fe}_3\text{O}_4$ ratio was caused by increase of corrosion potential as a result of increase in DO concentration. These results are consistent with the fact that the stable oxide is changed from Fe_3O_4 to Fe_2O_3 in higher corrosion potential on Pourbaix diagram of Fe- H_2O at 573 K [8].

Figure 8 shows the weight changes of coupon type specimen and rotated disk specimen plotted as a function of the $\text{Fe}_2\text{O}_3/\text{Fe}_3\text{O}_4$ ratio. The weight change of coupon type specimen shows almost constant, while that of rotated disk specimen decrease with increasing the $\text{Fe}_2\text{O}_3/\text{Fe}_3\text{O}_4$ ratio. Additionally, the weight changes of coupon type specimen and rotated disk specimen showed no significant difference when $\text{Fe}_2\text{O}_3/\text{Fe}_3\text{O}_4$ ratio reached 2.

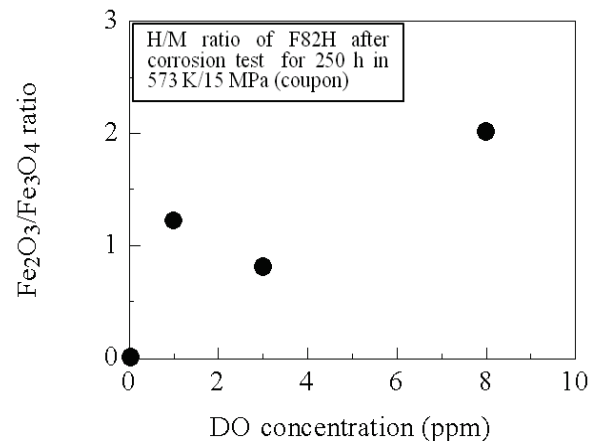
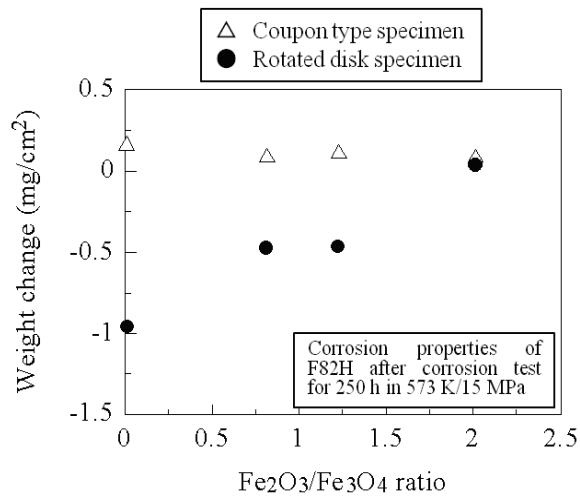


Figure 7 Hematite/Magnetite ratio plotted as a function of DO concentration.



[8] B. Beverskog *et al.*, Corrosion Science. **38**, 2121-2135 (1996).

Figure 8 Relationship between the weight changes of coupon type specimen and rotated disk specimen and Hematite/Magnetite ratio.

That is to say, the formation of Fe₂O₃ is effective for the corrosion in flowing high temperature pressurized water, and the effect of water flow is negligible when Fe₂O₃/Fe₃O₄ ratio reached about 2.

4. Conclusion

1. The significant weight loss by water flow was observed except for the test in the water with DO 8 ppm. It becomes significant with lowering DO concentration.
2. The weight loss of rotated disk specimen was seemed to be attributable to dissolution of Fe ion, which caused by dissolution and/or exfoliation of Fe₃O₄.
3. Fe₂O₃ may acts as a diffusion barrier of Fe ion transport. Therefore, it seemed that the formation of Fe₂O₃ was effective for the suppression of weight loss, and it is considered that the effect of water flow is negligible when Fe₂O₃/Fe₃O₄ ratio reached about 2.

References

- [1] M. Akiba *et al.*, Fusion Engineering and Design **85**, 1766-1771 (2010).
- [2] T. Hirose *et al.*, Fusion Engineering and Design **86**, 2265-2268 (2011).
- [3] Y. Nomoto *et al.*, Fusion Engineering and Design **81**, 719-724 (2006).
- [4] K. Shiba *et al.*, JAERI-Tech 97-038 (1997).
- [5] T. Hirose *et al.*, Journal of Nuclear Materials **367-370**, 1185-1189 (2007).
- [6] A. Suzuki *et al.*, J. Plasma Fusion Res. **86**, 390-392 (2010).
- [7] H. Abe *et al.*, Journal of the Surface Finishing Society of Japan **63**, 290-295 (2012).